On the inner disc structure of MWC480: evidence for asymmetries?

N. Jamialahmadi, B. Lopez, P. Bério, A. Matter, S. Flament, H. Fathivavsari, T. Ratzka, M. Sitko, A. Spang, R. Russell

Monthly Notices
of the
ROYAL ASTRONOMICAL SOCIETY

MNRAS **473,** 3147–3157 (2018)
Advance Access publication 2017 September 28

doi:10.1093/mnras/stx2533

On the inner disc structure of MWC480: evidence for asymmetries?

N. Jamialahmadi,[1,2,3★] B. Lopez,[3★] Ph. Berio,[3] A. Matter,[3] S. Flament,[3] H. Fathivavsari,[1] T. Ratzka,[4] M. L. Sitko,[5,6] A. Spang[3] and R. W. Russell[7]

[1]*School of Astronomy, Institute for Research in Fundamental Sciences (IPM), P.O. Box 19395-5746, Tehran, Iran*
[2]*European Southern Observatory, Karl-Schwarzschild. str. 2, D-85748 Garching, Munich, Germany*
[3]*Laboratoire J.-L. Lagrange, UMR 7293, University of Nice Sophia-Antipolis, CNRS, Observatoire de la Cote D'Azur, Boulevard de l'Observatoire – CS 34229 – F-06304 NICE Cedex 4, France*
[4]*Institute for Physics / IGAM, NAWI Graz, Karl-Franzens-Universität, Universitätsplatz 5/II, A-8010 Graz, Austria*
[5]*Department of Physics, University of Cincinnati, Cincinnati, OH 45221, USA*
[6]*Space Science Institute, 4750 Walnut Street, Boulder, CO 80303, USA*
[7]*The Aerospace Corporation, Los Angeles, CA 90009, USA*

Accepted 2017 September 26. Received 2017 September 26; in original form 2017 March 14

ABSTRACT

Studying the physical conditions structuring the young circumstellar discs is required for understanding the onset of planet formation. Of particular interest is the protoplanetary disc surrounding the Herbig star MWC480. The structure and properties of the circumstellar disc of MWC480 are studied by infrared interferometry and interpreted from a modelling approach. New observations are driving this study, in particular, some recent Very Large Telescope Interferometer (VLTI)/MIDI data acquired in 2013 December. Our one-component disc model could not reproduce simultaneously all our data: the spectral energy distribution, the near-infrared Keck Interferometer data and the mid-infrared data obtained with the MIDI instrument. In order to explain all measurements, one possibility is to add an asymmetry in our one-component disc model with the assumption that the structure of the disc of MWC480 has not varied with time. Several scenarios are tested, and the one considering the presence of an azimuthal bright feature in the inner component of the disc model provides a better fit of the data.

Key words: instrumentation: interferometers – techniques: interferometric – planetary systems – protoplanetary discs – circumstellar matter.

1 INTRODUCTION

Herbig Ae/Be (HAeBe) stars are intermediate-mass, pre-main-sequence stars (PMS) characterized by the presence of emission lines (Jamialahmadi et al. 2015) and an infrared (IR) excess over the stellar photosphere emission. The observed IR excess is caused by circumstellar dust confined to a disc. The study of the structure and physical conditions in such a disc is of great interest for gaining a better understanding of how planetary systems, like our own, are formed.

MWC480, is a Herbig/Ae star (HD 31648, *A*2/3ep + sh), with a mass of 1.67 ± 0.07 $M_{\odot}$ (Simon, Dutrey & Guilloteau 2000). It is located at $d = 137 \pm 31$ pc (van Leeuwen 2007). This star is one of the brightest Herbig Ae stars at millimetre(mm) wavelengths (Mannings, Koerner & Sargent 1997). The 1.4-mm thermal continuum emission map, obtained with the IRAM telescopes (Simon et al. 2000; Piétu et al. 2006) shows a protoplanetary disc with a major axis of 1.20 ± 0.15 arcsec (FWHM), corresponding to a half-maximum size ∼85 ± 20 au. However, the radius of the mm dust disc of MWC480 is estimated to be 200 au based on ALMA observations (Huang et al. 2017).

The dusty disc does not show strong large-scale asymmetries, except a putative emission feature extending to the south (Sandell, Weintraub & Hamidouche 2011) and nearly aligned with a jet-like emission observed by Hamidouche, Wang & Looney (2006). Large mm grains seem to dominate the sub-mm and mm emission (Sandell et al. 2011) while radial variations of the dust grain size distribution were also detected with a dust emissivity index increasing with radius (Guilloteau et al. 2011). In parallel, the global structure of the gaseous disc, observed in various CO lines, seems to be typical of a disc with continuous surface density distribution evolving by angular momentum transfer through viscous diffusion (Akiyama et al. 2013). These findings point to a continuous disc with a globally axisymmetric structure at large scale both in gas and dust. Huang et al. (2017) presented ALMA observations at 0.6 arcsec resolution of molecules DCO^+, $H^{13}CO^+$, DCN and $H^{13}CN$ in a disc with continuous surface density distribution around MWC480. They found that the $H^{13}CO^+$ and DCO^+ radial emission profiles peak at 40 au and the H^+CN profile is centrally peaked. Although the DCN

★ E-mail: nari.jami@gmail.com (NJ); bruno.lopez@oca.eu (BL)

emission was weak, it was consistent with the Keplerian rotation pattern established by the other three lines observed. The DCN emission appeared to feature a central dip, but the signal-to-noise ratio was too low to be definitive. Therefore, the axisymmetric structures were seen in both in gas and dust at ALMA observations.

However, does this apparent axisymmetric and continuous structure translate to smaller scales in the inner disc regions (planet-forming regions)? Can we expect faster and differentiated evolution, with already signposts of disc clearing, in the 0.1–10 au inner region? First hints came from Sitko et al. (2008), who highlighted an IR variability possibly related to a time-dependent shadowing of outer disc areas by the inner disc, knowing that MWC480 is still actively accreting.

Such time-dependent shadowing is supported by a marginally scattered-light detection of the disc by Grady et al. (2010), followed by another detection in scattered polarized light at a time the NIR excess was historically low (Kusakabe et al. 2012). Since no temperature change was observed at that time, this drop in NIR emission thus very likely correlated with the scaleheight variability of the inner rim of the dust disc. Spatially resolving the inner 0.1–10 au inner disc is thus the key to unveil the origin of this shadowing and more generally the possibility of a differentiated evolution between the inner and outer disc regions. IR stellar interferometry is so far the only technique capable of reaching the angular resolution level of a few milliarcseconds which translates to sub-au scales at the distance of MWC480. However, only sparse interferometric data have been obtained on MWC480. Using the Keck Interferometer, Eisner et al. (2009) and Eisner, Hillenbrand & Stone (2014) spatially resolved the innermost dust and hot gas disc. In particular, they showed that the Brackett gamma line emission originated mostly inside the dust sublimation radius (<0.1 au) probably in accretion columns and/or shocks. Moreover, the only MIR interferometric measurement obtained with the VLTI/MIDI was modelled independently by Menu et al. (2015) and Jamialahmadi et al. (2014). Using axisymmetric models, they both showed that most of the MIR continuum emission from warm dust originates within 1–10 au. Given the very low number of interferometric observations (one with the VLTI and one with the KI), the putative axisymmetric structure of the inner regions needs to be confirmed with additional measurements obtained along other baseline directions.

In this context, the aim of this paper is to provide a more detailed description of the inner disc. In particular, we aim to assess the axisymmetric structure of the IR emitting region by combining the existing IR interferometric observations with new MIDI measurements obtained in 2013 in a perpendicular direction. This new measurement is thus a key to reinforce, or not the possibility of an axisymmetric inner disc, and unveil signs of ongoing physical processes.

Section 2 of this paper summarizes the observations and the data processing. Section 3 shows the results of the interferometric observations. Section 4 describes our semi-analytical models, and the related results. Section 5 includes a discussion on the modelling results and Section 6 summarizes our work and outlines some observational perspectives to validate the existence of azimuthal asymmetries in the discs.

2 OBSERVATIONS

2.1 MIDI observations

MWC480 was observed in 2007 and in 2013 with the instrument MIDI of the VLTI (Leinert et al. 2003) of the ESO Paranal Observatory. The first observation was carried out on 2007 February 4 using two 8-m unit telescopes (UTs). The second observation was made on 2013 December 29 using two 1.8-m auxiliary telescopes (ATs). The observations were performed using the prism as dispersive element giving a spectral resolution of $R \sim 30$ in the N band for the wavelength range 8–13 μm using the HIGH-SENS mode. Photometry measurement (total flux) and visibility (normalized coherent flux) were obtained for each observation. A summary of the observing log, containing the length of the projected baselines is shown in Table 1. The UV coverage of all the interferometric observations is shown in Fig. 1 (top).

Table 1. Log of long baseline interferometry observations. Our recent MIDI/VLTI observations with ATs (P.I.: Ratzka) were conducted in 2013 December. Past observations were also made with the MIDI instrument (P.I.: Di Folco) and with the Keck Interferometer (Eisner et al. 2009).

Instrument	Date	Telescopes and baselines	B_p (m)	P.A. (°)
MIDI	2007-02-04	UTs: UT2-UT3	42.8	52°
HIRES	2007-07-03	Keck1-Keck2	84.9	48°
MIDI	2013-1-29	ATs: K0-J3	28.6	330°

The MIDI data reduction was carried out using the EWS (Expert Workstation) software package. EWS performs a coherent analysis of dispersed fringes to estimate the complex visibility of the source. The method and the different processing steps are described in Jaffe (2004). The calibrated visibilities were then obtained by dividing each raw visibility measurement by the instrumental visibility measured on the closest calibrator in time.

In order to calibrate the visibilities of the science source in 2007 and 2013, we used the calibration star HD 20644. This calibrator was selected from the SearchCal tool from the JMMC.[1]

As we can see in Fig. 1 (middle-left), representing the visibility in 2007, the source is barely resolved (visibility level of about 0.8) and shows a flat visibility profile across the N band. In contrast, the MIDI visibility obtained in 2013 with a shorter perpendicular baseline, varies from 0.7 to 0.5 across the N band. This visibility drop stands out in spite of larger error bars due to sensitivity reasons since this visibility was obtained with the smaller ATs.

MWC480 was also observed with the Keck Interferometer in the K band in the wavelength range 2.08–2.33 μm (Eisner et al. 2009). We downloaded the reduced data from the Keck Archive. According to Fig. 1 (bottom-left), the peak in the data, which has higher visibility, is related to the Br γ emission at 2.165 μm.

2.2 Spectroscopic observations with SpeX

We observed MWC480 with the SpeX spectrograph on IRTF in parallel to the most recent MIDI observations. The SpeX observations were carried out on 2013 September 11 using the cross-dispersed (hereafter XD) echelle gratings in both short-wavelength mode (SXD) covering 0.8–2.4 μm and long-wavelength mode (LXD) covering 2.3–5.4 μm (Rayner, Cushing & Vacca 2009). On nights where the seeing is 1 arcsec or better, this technique yields absolute fluxes that agree with aperture photometry to within 5 per cent or better (Ingleby et al. 2015). Since our observations were performed with a seeing of 1 arcsec, we estimate the SpeX absolute photometric calibration uncertainty to be 5 per cent.

The data were reduced using the SPEXTOOL software (Vacca, Cushing & Rayner 2003; Cushing, Vacca & Rayner 2004).

[1] http://www.mariotti.fr/

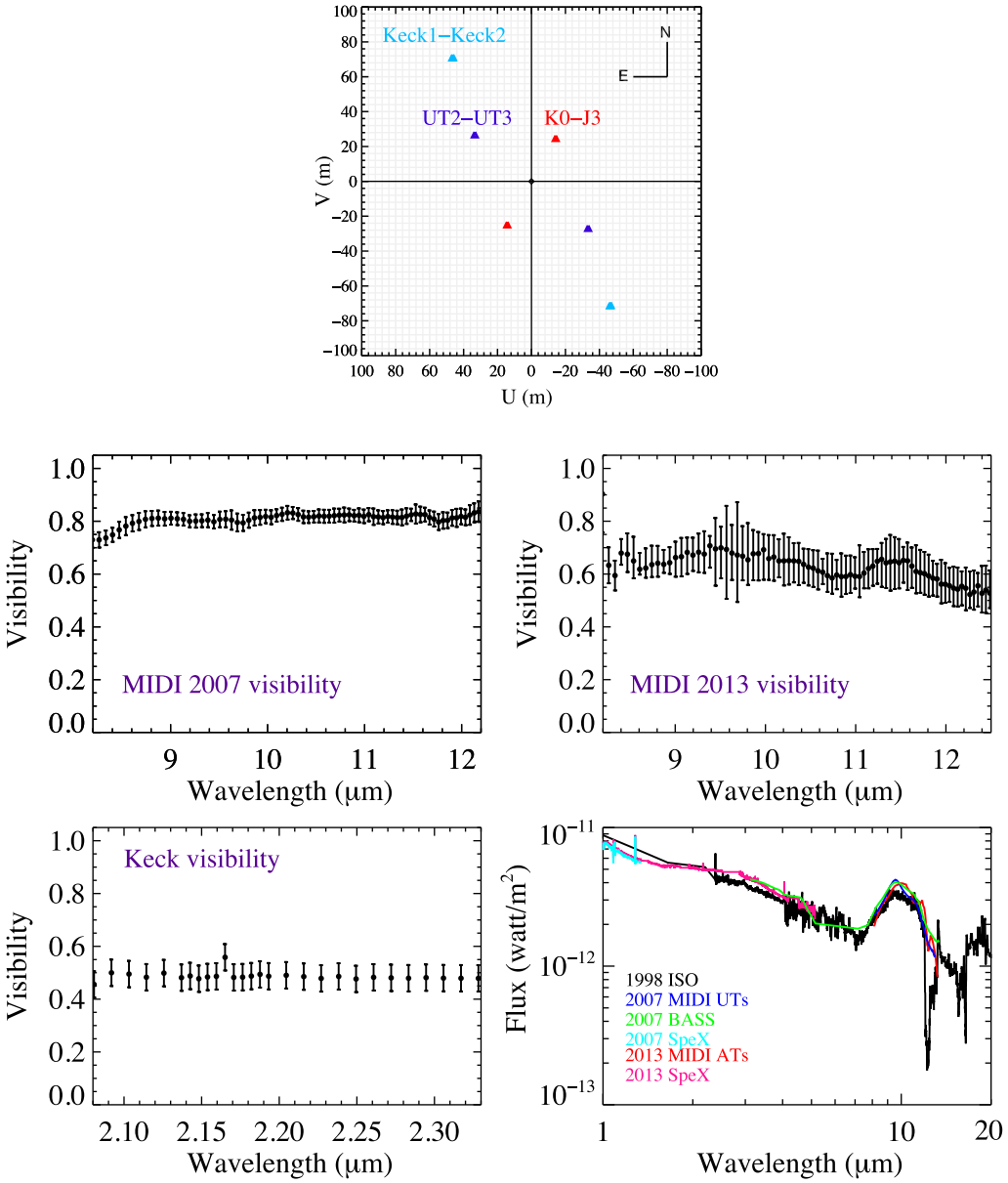

Figure 1. Top: UV coverage for the three sets of interferometric observations. Middle-left: measured *N*-band visibility of MWC480 as a function of wavelength in 2007 with spectral resolution of $R = 30$. Middle-right: measured *N*-band visibility of MWC480 as a function of wavelength in 2013 with spectral resolution of $R = 30$. Bottom-left: measured *K*-band visibility of MWC480 (the error bars are represented for few points only). Bottom-right: ISO data for wavelengths 1–20 μm in 1998 (black colour), SpeX data for wavelengths 1–5.4 μm (cyan colour) and BASS data for wavelengths 5.5–14 μm in 2007 (green colour), SpeX data for wavelengths 1–5.4 μm in 2013 (pink colour), the MIDI total flux for wavelengths 8–13.5 μm in 2007 (blue colour) and in 2013 (red colour).

Existing SpeX data from 2007 by Sitko et al. (2007) was used to cover the epoch of the first MIDI measurement.

According to Fig. 1 (bottom-right), the 2007 and 2013 MIDI total flux measurements do not present any significant change in amplitude. Moreover, they both appear consistent with the other mid-IR measurements obtained in the same respective epochs, i.e. the SpeX and BASS[2] data. Even the ISO[3] spectrum obtained in 1998 appeared very similar.

[2] http://irtfweb.ifa.hawaii.edu/Facility/
[3] http://irsa.ipac.caltech.edu/data/SWS/

Between 2007 and 2013, the NIR and MIR variability do not appear anyway more than 10 per cent. Interestingly, this relative error is what we estimated for the absolute calibration error of our MIDI data and is greater than what we estimated for the absolute calibration error of our SpeX data.

3 MODELLING

To interpret all our measurements in a consistent way, i.e. the SED, the Keck visibility and the MIDI visibilities, we developed a semi-analytical model.

Our model is based on the hypothesis of a temperature and surface density-gradient for the circumstellar disc comparable to what was used for previous disc descriptions (e.g, Hillenbrand & Hartmann 1998). Such a disc model is defined by an inner radius $r_{\rm in}$ and an outer radius $r_{\rm out}$, with temperature and surface density profiles that are parametrized by power laws:

$$T_r = T_{\rm in}\left(\frac{r}{r_{\rm in}}\right)^{-q}, \tag{1}$$

$$\Sigma_{\rm r} = \Sigma_{\rm in}\left(\frac{r}{r_{\rm in}}\right)^{-p}, \tag{2}$$

with q ranging from 0.5 (flared irradiated discs) to 0.75 (standard viscous disc or flat irradiated discs), see e.g. Pringle (1981). $T_{\rm in}$ is the temperature of a free grain[4] located at $r = r_{\rm in}$ which is the inner radius of the disc.

Equating the absorption and the emission of a grain with non-chromatic (grey) absorptivity, one can calculate the $T_{\rm in}$ at $r_{\rm in}$ in equation (1):

$$T_{\rm in} = T_{\star}\left(\frac{R_{\star}}{2r_{\rm in}}\right)^{\frac{1}{2}}, \tag{3}$$

where T_* (= 8970 K) and R_* (= 0.068 mas) are the stellar effective temperature and the stellar radius, respectively.

In the models of Dullemond, Dominik & Natta (2001) and Chiang & Goldreich (1997), $\Sigma_{\rm in}$ has been considered at $r = 1$ au, while in, e.g. Dutrey et al. (1998), Dutrey et al. (2011), who used mm observations, $\Sigma_{\rm in}$ is assumed to be defined from the outer radius of the disc. $\Sigma_{\rm in}$ is related to the total mass amount of the dust. The mass of the dust is given by

$$M_{\rm dust} = \int_0^{2\pi}\int_{r_{\rm in}}^{r_{\rm out}} \Sigma_{\rm r} r\, {\rm d}r{\rm d}\theta \tag{4}$$

Combining equations (2) and (4) gives

$$\Sigma_{\rm in} = \frac{M_{\rm dust}}{2\pi r_{\rm in}^{p} f}, \tag{5}$$

where

$$f = \frac{1}{2-p}\left[\left(\frac{r_{\rm out}}{r_{\rm in}}\right)^{2-p} - 1\right] \tag{6}$$

p value in the equation (2) varies in different studies. Isella, Carpenter & Sargent (2009) show that p ranges from −0.8 to 0.8 based on observations of low- and intermediate-mass PMS stars. Assuming constant mass accretion rate at constant viscosity p value is 1. p is assumed to be 1.5 for the MMSN (minimum mass solar nebula) (Weidenschilling 1997) and assumed often as a basis in other disc models (e.g. Chiang & Goldreich 1997; Dullemond et al. 2001; Eisner et al. 2009). p is assumed not to be 2 in our models.

In our disc model, the observer receives for each disc elementary surface area A:[5]

$${\rm d}F_{\lambda}(i) = B_{\lambda}\left[T(r)\right]\left[1 - \exp\left(-\frac{\tau_{\lambda}(r)}{\cos(i)}\right)\right]\left(\frac{A}{D^2}\right), \tag{7}$$

where, i is the disc inclination and the quantity A/D^2 represents the solid angle of each elementary surface area as seen at the distance D. $\tau_{\lambda}(r) = \Sigma(r) \times \kappa_{\lambda}$ represents the optical depth in the vertical direction, with κ_{λ} the mass absorption coefficient. For the latter, we used κ_{λ} from Thi, Woitke & Kamp (2011), which is computed from Mie theory. They considered a power law (proportional to $a^{-3.5}$) for the grain size distribution with a minimum size of $a_{\rm max} = 0.02$ μm and three values for the maximum size of $a_{\rm max} = [10, 50, 200]$ μm.

The interstellar dust optical constants of Laor & Draine (1993) for amorphous grains are considered.

The stellar contribution is represented in our model by $B_{\lambda}(T_*) \times (\pi\, {\alpha_*}^2)$. Here, $\alpha_* = R_*/D$ is the stellar angular radius.

To take into account the Br γ emission line present in our K-band data, we modelled circumstellar Br γ emission at 2.165 μm by including a narrow optically thin isothermal gaseous disc in the inner region of the disc. We based our modelling of the Br γ emission on the study done by Eisner et al. (2009).

After creating the image of the disc, which is the sum of the flux of the central star and the disc for each disc elementary surface area, one can calculate the visibility for each wavelength. We do the Fourier transform of the image at each wavelength and the visibility is the modulus of the Fourier transform divided by the total flux, which is equal to the Fourier transform at zero spatial frequency.

3.1 Axisymmetric model

As a first step, we model the inner disc of MWC480 with an axisymmetric one-component disc with a continuous radial structure. Eisner et al. (2007) already tried to model the IR excess of this source assuming an optically thick disc emission. However, such a model could not account for all the IR excess between 2 and 10 μm. In our case, we rather use a disc model that includes radial temperature and surface density profiles (see equations 1 and 2). Our model thus takes into account the disc vertical optical depth towards the observer. To limit the number of free parameters, the inner radius is fixed to 0.27 au (Eisner et al. 2009). Since our study focuses on the NIR and MIR emission, which comes mainly from 0.1 to 10 au of the disc (Menu et al. 2015), we set the outer radius of the disc to 20 au. Reproducing longer wavelength emission is out of the scope of this article. The inclination and the position angle of the disc are also fixed to $i = 37^{\circ}$ and PA = 140°, respectively (Chapillon et al. 2012 and Piétu, Dutrey & Guilloteau 2007). As we mentioned in Section 3, we adopted the grain size distribution used by Thi et al. (2011) with a minimum size of $a_{\rm max} = 0.02$ μm and a maximum size of $a_{\rm max} = 10$ μm.

The free parameters of the one-component disc model are thus:

(i) the temperature power-law exponent q,
(ii) the surface density power-law exponent p,
(iii) the dust mass $M_{\rm dust}$.

In order to obtain the best-fitting model, first we scanned a wide range of values for each parameter and minimized the global χ^2 between the model and the observations. The χ^2 maps were obtained for the SED, the MIDI and the Keck visibilities as following:

$${\chi^2}_{\rm SED} = \sum_{i=1}^{N_{\rm SED}} \frac{(F_{\rm model}(\lambda_i) - F_{\rm obs}(\lambda_i))^2}{{\sigma^2}_{F_{\rm obs}(\lambda_i)}} \tag{8}$$

$${\chi^2}_{\rm vis1} = \sum_{k=1}^{n_{\rm baseline}} \sum_{j=0}^{N_{\rm visMIDI}} \frac{(V_{\rm model}(\lambda_j, B_k) - V_{\rm MIDI}(\lambda_j, B_k))^2}{{\sigma^2}_{\rm vis(\lambda_j)}} \tag{9}$$

[4] A grain illuminated directly by the central star assuming no radiative exchange with other grains.
[5] The elementary surface area of the disc is defined by our pixel size in the simulated brightness maps of our model.

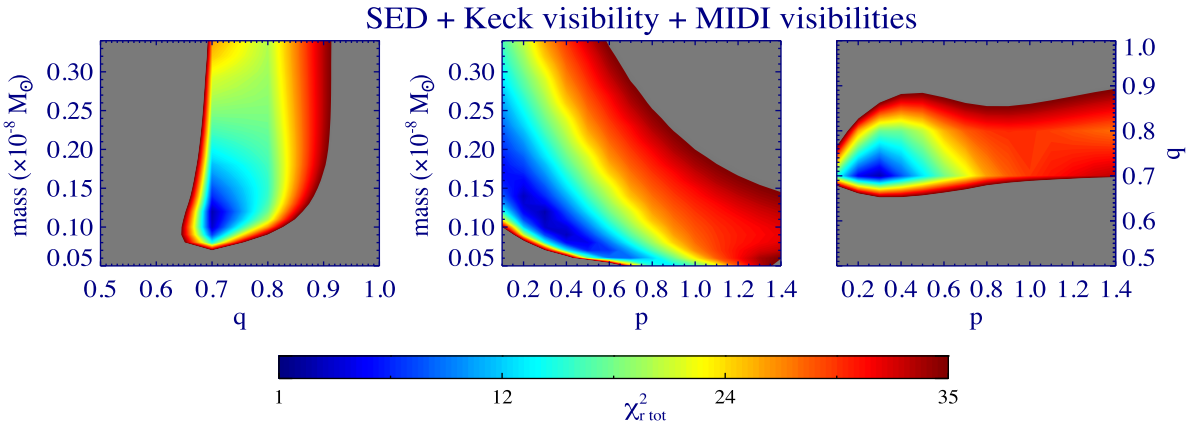

Figure 2. Minimum χ^2maps for the SED, the Keck visibility and the MIDI visibilities for the one-component disc model. We show the minimum χ^2 for each pair of parameters. The grey areas are related to the χ^2 larger than 35.

Table 2. Scanned parameter range of one-component disc model and the best-fitting values for each parameter. The 1σ uncertainties on the parameters have been shown as well.

Scan range	p	q	$M_{\rm dust}$ [$M_\odot$]	$n_{\rm steps}$
Wide	[0.1–1.5]	[0.1–1.5]	[0.01–0.5] $\times 10^{-8}$	30
Narrow	[0.1–0.6]	[0.5–0.9]	[0.05–0.2] $\times 10^{-8}$	15
Best fit	0.3 ± 0.08	0.7 ± 0.02	$(0.11 \pm 0.03) \times 10^{-8}$	

$$\chi^2_{\rm vis2} = \sum_{l=0}^{N_{\rm visKeck}} \frac{(V_{\rm model}(\lambda_l) - V_{\rm Keck}(\lambda_l))^2}{\sigma^2_{\rm vis(\lambda_l)}} \quad (10)$$

$$\chi^2_{\rm tot} = \chi^2_{\rm SED} + \chi^2_{\rm vis1} + \chi^2_{\rm vis2} \quad (11)$$

$$\chi^2_{r\ \rm tot} = \frac{\chi^2_{\rm tot}}{(N_{\rm SED} + N_{\rm visMIDI} \times n_{\rm baseline} + N_{\rm visKeck} - 3)} \quad (12)$$

For the SED fitting, we used ISO data in 1998 and considered the wavelength range between 3 and 13 μm. For the MIDI visibilities, we considered the wavelength range between 8.2 and 12.5 μm. For the Keck visibility, we considered the wavelength range between 2.08 and 2.33 μm. Fig. 2 illustrates the χ^2 maps for the best parameters. A minimum χ^2 can be identified in the maps. The value of the $\chi^2_{r\ \rm tot}$ for the wide range of parameters was 1.38. In a second step, we scanned on a narrower range around the global minimum χ^2 to refine the best-fitting model and the estimation of the best-fitting parameters. Table 2 shows the wide and narrow value ranges that were scanned for every parameter. The uncertainties of the best parameters were derived using a Monte Carlo procedure. To this aim, assuming a normal error distribution, 1000 random data sets corresponding to the measured values varied among their 1σ uncertainties were simulated. In the next step, calculating the standard deviation of each best-fitting parameter value matching the simulated data sets, one could derive the uncertainties on the parameters (see Table 2).

Using the best-fitting parameter values we derived for the one-component disc model, we plot our measurements in Fig. 3. The SED is mostly up to 8 μm, the Keck visibility and the 2007 MIDI visibility are reasonably well reproduced, as already shown by Jamialahmadi et al. (2014). However, our best-fitting model cannot explain well the 2013 MIDI visibility and the SED between 8 and 13 μm. We obtained this best-fitting model using a maximum grain size of 10 μm, which is consistent with the silicate grain emission features. We plot the synthetic image of MWC480 at $\lambda = 10$ μm (Fig. 3, bottom).

As a caveat, we remind that equation (7) does not include a distinct term for the continuum emission, which implies that our model aims to reproduce both the IR continuum and the silicate emission band. As a consequence, $M_{\rm dust}$ should be seen as a scaling factor for the IR emission level rather than a pure estimation of the actual mass of dust in the inner disc. Moreover, the corresponding vertical optical depth is always less than 1 (see Fig. 4). Therefore, the disc is far from being optically thick in the IR. If one is interested in adding far-IR emissions to the near and mid-IR regions, indeed in that case, one needs to model the disc mid-plane where larger grains accommodate and are responsible for the far-IR emissions. Therefore, in that case we may have better estimation of the mass of the disc. However, we remind that the scope of this paper is to model the IR emission coming from the inner disc.

3.1.1 *Time variable models*

As mentioned in Section 2.2, the mid-IR spectra taken at two epochs in 2007 and 2013 are consistent with each other within their uncertainties. This fact gives us a possibility to assume that the structure of the disc of MWC480 has not varied in 2007 and 2013. However, in order to exclude the temporal variability as the source of changes in the visibilities in these 2 yr, one should demonstrate that fitting independently the two MIDI epochs would produce a photometric variability that is inconsistent with the observed mid-IR spectra, which is dominated by the silicate emission. To this aim, we tried to explore the free parameters of p, q and $M_{\rm dust}$ to find the best model, which can fit the MIDI visibility in 2013. We followed the same method used in Section 3.1 to calculate the χ^2 fitting process and the uncertainties of the parameters. Contributing the SED, the Keck visibility and the MIDI visibility in 2007 in the χ^2 fitting process were not effective to obtain the best-fitting MIDI visibility in 2013. Consequently, we included only the MIDI visibility in 2013 in the χ^2 fitting process to obtain the best-fitting parameters values. Table 3 shows the best-fitting parameters and their uncertainties. Fig. 5 illustrates the best-fitting model, which can fit only the MIDI visibility in 2013 but not the SED, the Keck and the MIDI visibility in 2007 simultaneously.

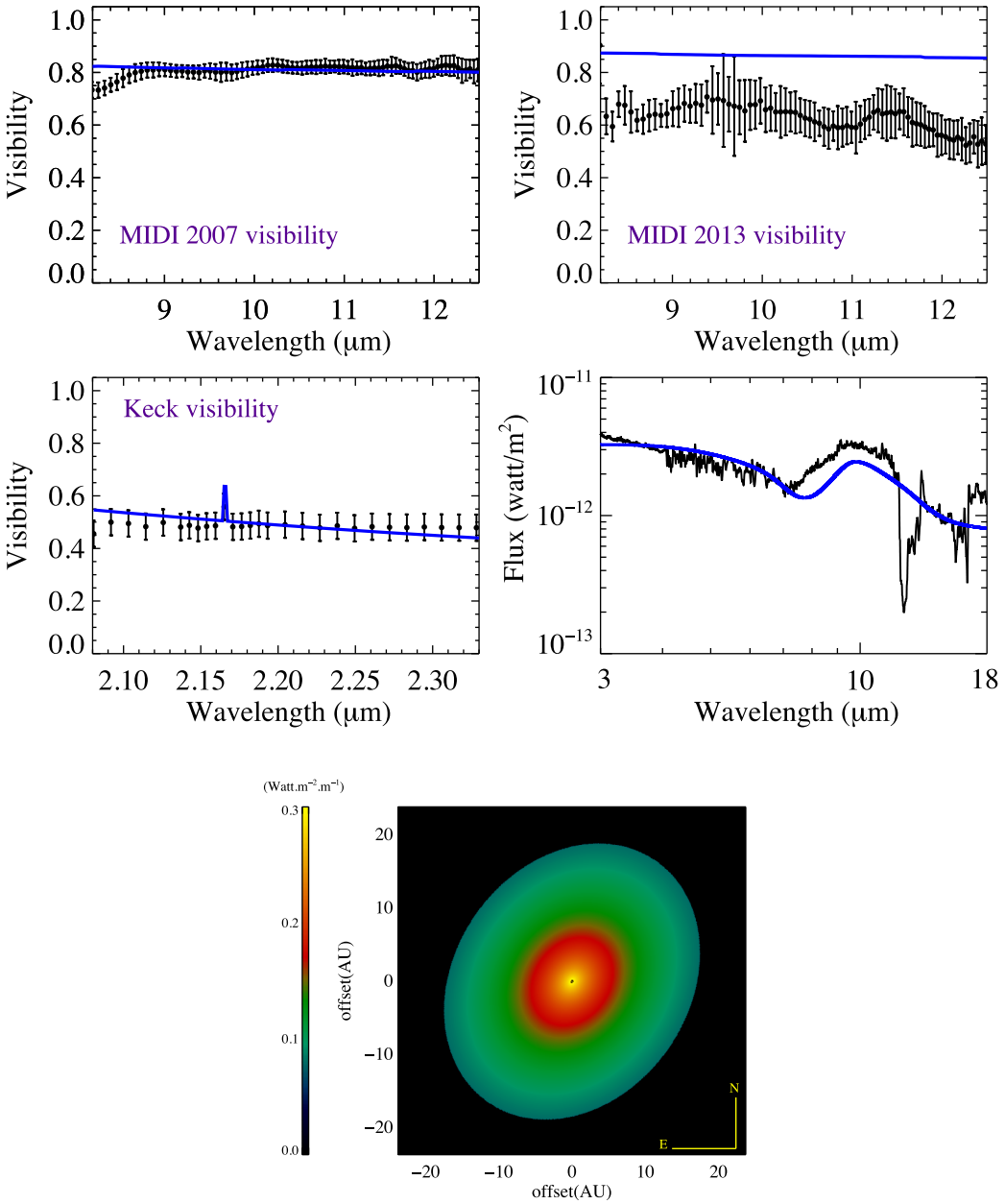

Figure 3. One-component disc model. Top: the MIDI visibilities in 2007 and 2013. Middle-left: the Keck visibility. Middle-right: the SED from 3 to 18 μm. The black lines in whole plots represent observations and the blue ones represent the best model. Bottom: the synthetic image of MWC480 at $\lambda = 10$ μm.

We then did a comparison between our best-fitting time-variable models which are consistent with the 2007 and the 2013 MIDI visibilities individually. In Fig. 6, we illustrate the time-variable models in 2007 and 2013 for the SED and the MIDI visibilities. The blue solid lines show the best-fitting model consistent with the MIDI visibility in 2007. In this model, we could reproduce the 2007 MIDI visibility and the SED but not the MIDI visibility in 2013 at the same time. The red solid lines show the model, which can explain the 2013 MIDI visibility but not the SED and the MIDI visibility in 2007. Indeed, our axisymmetric time-variable models produce the photometric variability that is inconsistent with the observed mid-IR spectra. This means that our assumption that the structure of the disc of MWC480 has not varied in 2007 and in 2013 based on their consistent MIDI spectra can be truly considered.

As a conclusion, an axisymmetric model, time-variable model or not, appears not to be anymore consistent with our data when taking into account the 2013 MIDI visibility. In the next section, we explore the possibility of an asymmetric disc model to reproduce our data set in a more consistent way.

3.2 Asymmetric model

With our axisymmetric model, we failed to reproduce the SED, the Keck and the MIDI visibilities simultaneously. For this reason, we consider in the following, the simplest situation that could produce azimuthal asymmetry, i.e. a bright feature in the disc.

Therefore, from our one-component disc model, we added a bright feature along the direction of the projected baseline of the

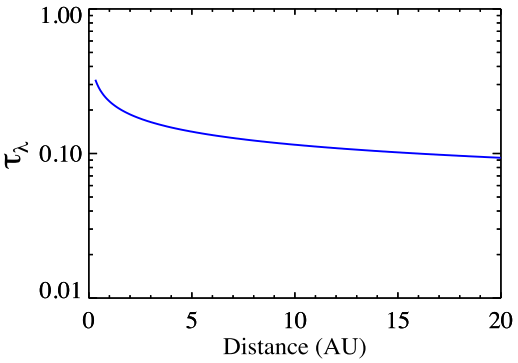

Figure 4. The vertical optical depth versus the distance from the central star.

Table 3. Scanned parameter range of one-component disc model for the best fit of MIDI visibility in 2013 and the best-fitting values for each parameter. The 1σ uncertainties on the parameters have been shown as well.

Scan range	p	q	$M_{\rm dust}$ [$M_\odot$]	$n_{\rm steps}$
Wide	[0.1–1.5]	[0.1–1.5]	[0.01–0.5] $\times 10^{-8}$	30
Narrow	[0.4–0.8]	[0.2–0.7]	[0.008–0.04] $\times 10^{-8}$	15
Best fit	0.6 ± 0.02	0.5 ± 0.03	$(0.01 \pm 0.006) \times 10^{-8}$	

2013 MIDI visibility. This choice is motivated by the fact that the clump should be invisible for the 2007 MIDI baseline (i.e. its projected distance on to the baseline direction is zero or close to zero). Our chosen azimuthal configuration for the clump enables that, without adding a temporal evolution of the azimuthal position of the clump in our model and therefore additional free parameters.

Such a feature could be an embedded companion or a local dust concentration in a clump. This bright feature or clump emission is modelled as an optically thick component having a blackbody emission $B_\lambda[T_{\rm cl}(d_{\rm cl})]$, where $T_{\rm cl}$ is the temperature of the clump and $d_{\rm cl}$ is the distance of the clump from the central star. For each surface area element of the clump, the observer receives

$$\mathrm{d}F_{\lambda,\rm clump} = B_\lambda\,[T_{\rm cl}(d_{\rm cl})]\left(\frac{A_{\rm cl}}{D^2}\right), \tag{13}$$

where $A_{\rm cl}$ is the elementary surface area of the clump which is defined by our pixel size in the simulated brightness maps of our model.

In this model, we set the best-fitting parameter values obtained for the one-component disc model as explained in Section 3.1. As mentioned above, the P.A. of the clump is set to the P.A. of the baseline used in 2013, i.e. 330° (see Table 1) to minimize the parameters of the clump. Therefore, the free parameters of the clump are following:

(i) the distance of the clump ($d_{\rm cl}$),
(ii) the size of the clump ($r_{\rm cl}$),
(iii) the temperature of the clump ($T_{\rm cl}$).

In order to obtain the best-fitting parameters, we carried out the same process as explained in Section 3.1 to reach the minimum χ^2. Fig. 7 illustrates the χ^2 maps for the best parameters. The value of the ${\chi^2}_{r\ \rm tot}$ for the wide range of parameters was 0.31. Table 4 shows the wide and narrow range of the values which were scanned for each parameter. The uncertainties of the parameters were derived as in Section 3.1. Fig. 8 presents the corresponding best-fitting MIDI

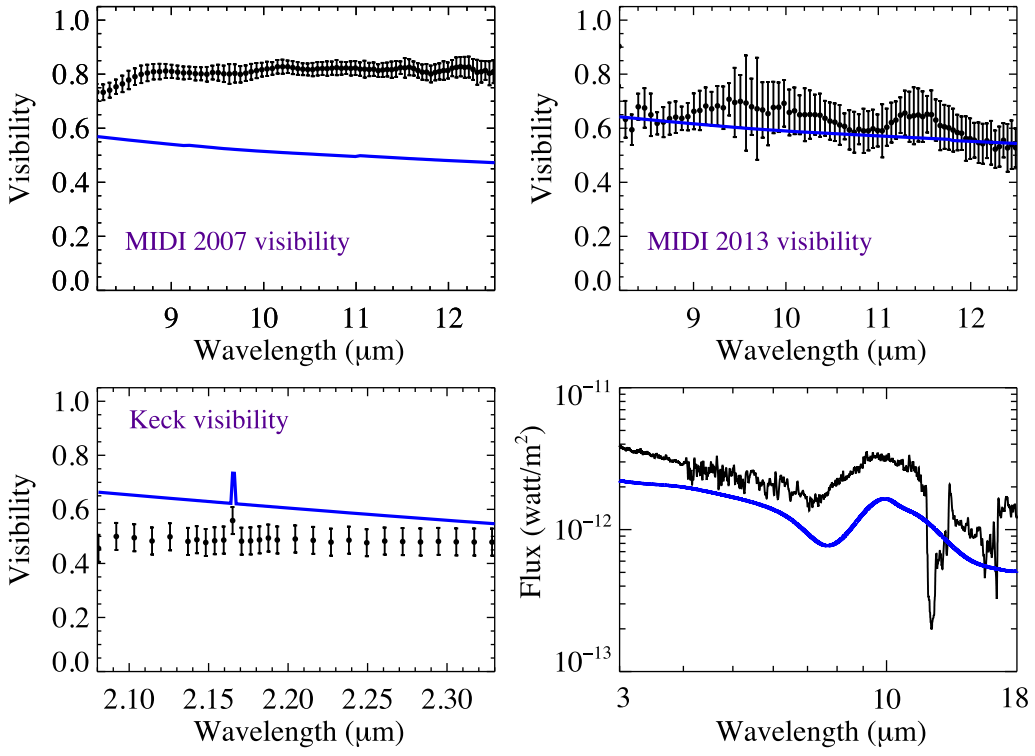

Figure 5. One-component disc model for the best fit of MIDI visibility in 2013. Top: the MIDI visibilities in 2007 and 2013. Bottom-left: the Keck visibility. Bottom-right: the SED from 3 to 18 μm. The black lines in whole plots represent observations and the blue ones represent the best model.

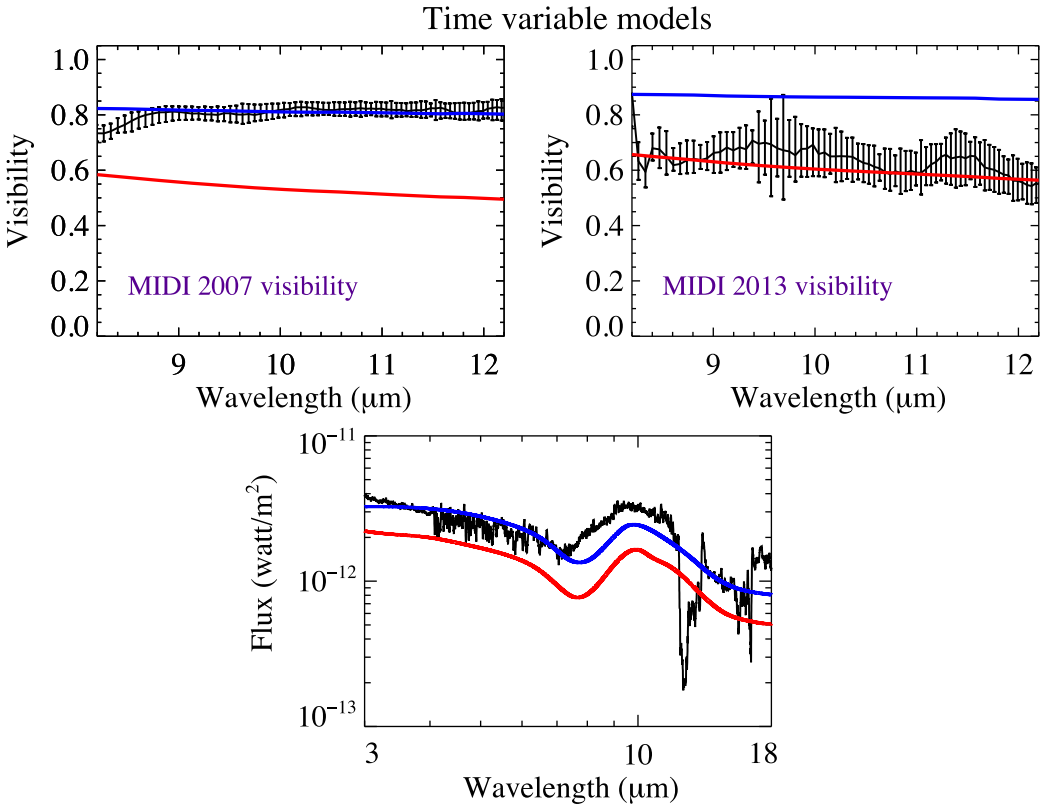

Figure 6. Time-variable models in 2007 and 2013. The blue solid lines are related to the best-fitting model, which reproduces the SED and the MIDI visibility in 2007 for the maximum grain size of 10 μm. The red solid lines are related to the model, which reproduces the MIDI visibility in 2013 for the maximum grain size of 10 μm.

visibilities and the SED, and the synthetic image for this best-fitting model at 10 μm.

The agreement with the 2013 MIDI visibility is now better. A partly resolved bright feature along the 2013 baseline direction allows us to decrease the visibility towards longer wavelengths. The agreement with the SED between 8 and 13 μm (silicate emission feature) is also better than in the axisymmetric case. All the other data are still consistently reproduced within their error bars.

In Fig. 9, we compared the photometry for the axisymmetric time variable models and the asymmetric model for the maximum grain size of 10 μm. We do show that the photometry changes in the time

Table 4. Scanned parameter range of the clump in the one-component disc model and the best-fitting values for each parameter. The 1σ uncertainties on the parameters have been shown as well.

Scan range	d_{cl} (au)	r_{cl} (au)	T_{cl} (K)
Wide	[1–10]	[0.1–2]	[100–1000]
Narrow	[4–7]	[0.6–1.2]	[300–500]
Best fit	5.45 ± 0.8	0.85 ± 0.12	400 ± 57

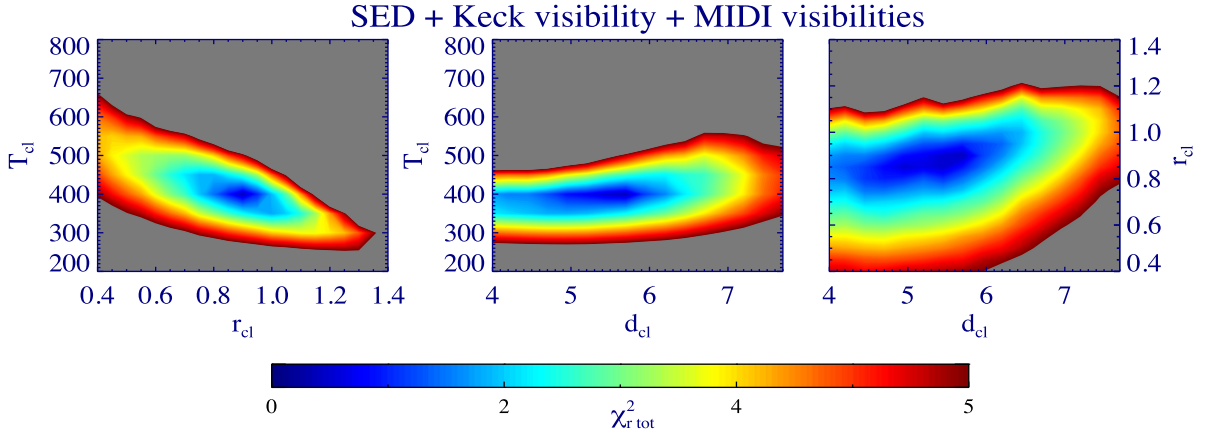

Figure 7. Minimum χ^2maps for the SED, the Keck visibility and the MIDI visibilities. We show the minimum χ^2 for each pair of parameters for the one-component disc model with the clump. The grey areas are related to the χ^2 larger than 5.

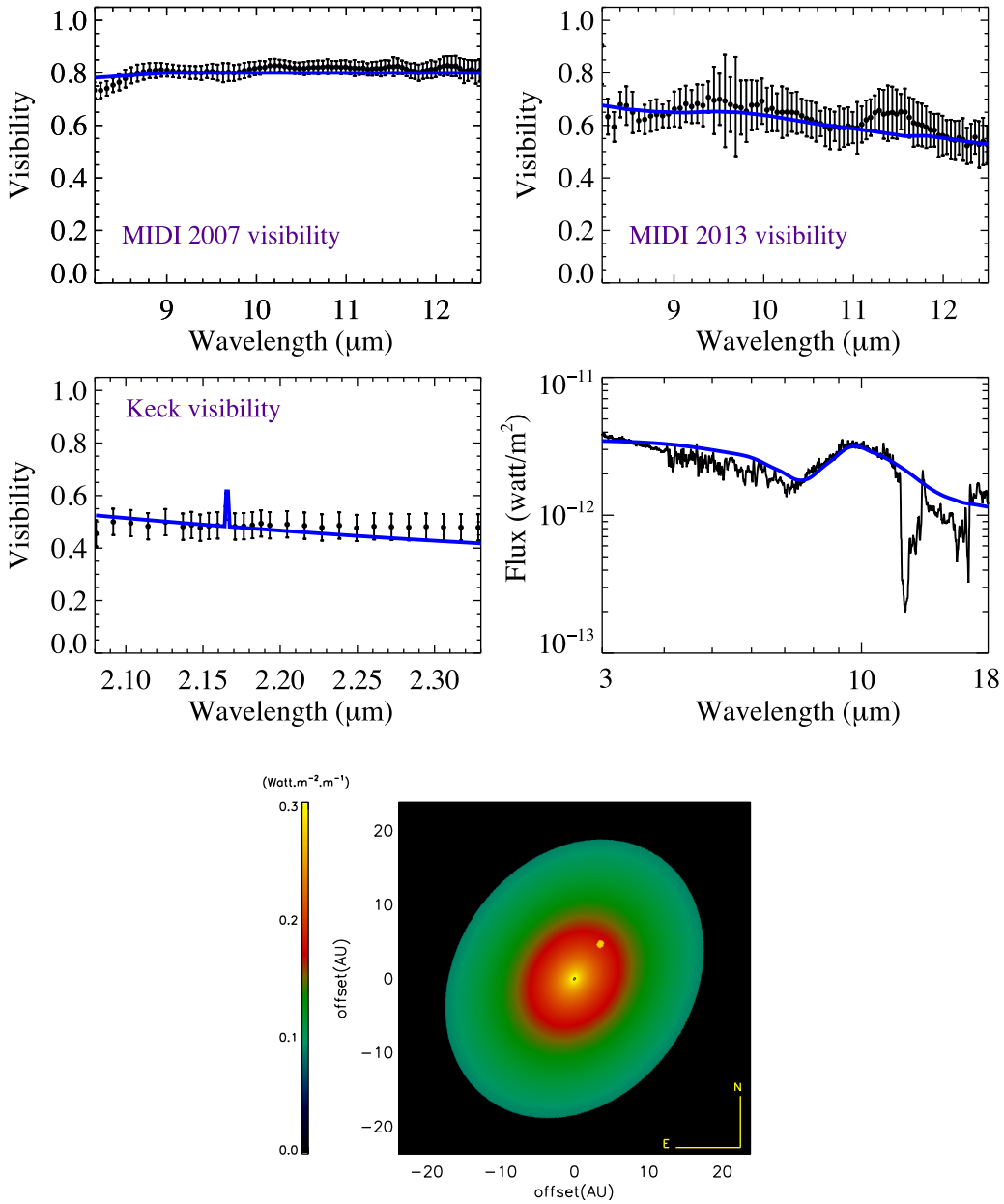

Figure 8. One-component disc model with a bright feature. Top: the MIDI visibilities in 2007 and 2013. Middle-left: the Keck visibility. Middle-right: the SED from 2 μm to 20 μm. The black lines in whole plots represent observations and the blue ones represent the best model. Bottom: the synthetic image of MWC480 at $\lambda = 10$ μm.

variable models is more significant than the changes between our best-fitting axisymmetric model discussed in Section 3.1 and the asymmetric one.

4 DISCUSSION

Our simultaneous modelling of the SED as well as the mid-IR interferometric data of MWC480 favours the possibility of an asymmetric inner disc. Indeed, a one-component disc model including a bright clump in the inner disc gives better agreement with our data set.

This assumes that the azimuthal location of the bright feature was either similar in 2007 and 2013, or such that the clump was invisible for the 2007 baseline (i.e. its distance projected on to the baseline direction is zero). We may thus wonder if it is consistent for instance with a clump of dust in Keplerian rotation around the central star. Since the derived distance of the clump, i.e. $d_{\rm cl} = 5.45 \pm 0.80$ au is a projected one, we need to retrieve the physical distance, i.e. the unprojected distance, which is $d_{\rm ucl} = 5.5 \pm 0.81$ au. Thus, we use this latter distance to calculate the orbital period of the clump using the following equation:

$$T = 2\pi\sqrt{\frac{r^3}{GM_\star}}, \tag{14}$$

where r is the unprojected distance of the clump ($d_{\rm ucl} = 5.5 \pm 0.81$ au) and M_* is the mass of the central star (1.67 ± 0.07 M$\odot$ Simon et al. 2000). With these parameters, the orbital period of

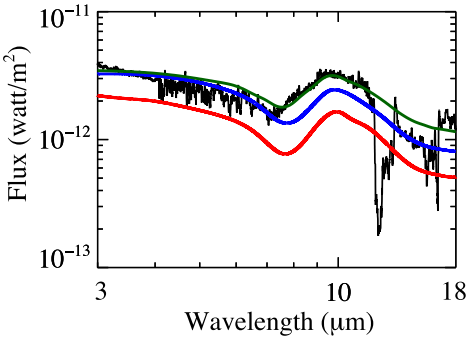

Figure 9. A comparison between the axisymmetric time variable models for 2007 and 2013 and the asymmetric model. The blue line is related to the best-fitting model, which reproduces the MIDI visibility in 2007 alone, the red line is related to the model, which reproduces the 2013 MIDI visibility alone, and the green line is related to the asymmetric model.

this bright feature would be 9.9 ± 2.1 yr, which is close to the time interval between the two MIDI observations, i.e. ∼7 yr.

The brightness ratio between the clump and its surroundings is nearly 6.5×10^2. This high brightness ratio results from the high optical depth of the clump compared to the very low optical depth of the disc at 5.45 au (the clump location of the model). The clump is assumed to be optically thick (see equation 13) while the disc optical depth is of the order of 4×10^{-3} at 10 μm and varies from 2×10^{-3} to 3×10^{-3} in the range 8–13 μm.

Binarity of the star can also cause an asymmetry in the disc. We tested this possibility with our models. In order to resolve the disc in the direction corresponding to the baseline orientation in 2013 and to decrease the visibility down to 0.6, we need a companion that is bright enough at the *N* band. However, such a stellar companion can be excluded since it would cause an additional NIR excess in the SED and an NIR visibility lower than the Keck one. Only a structure such as 'dusty clump' is cool enough to contribute mainly at MIR and longer wavelengths without increasing too much the NIR emission.

A disc warping or spiral waves can also make asymmetries in the disc. For instance, a disc warping was used by Kraus et el. (2013) to explain the asymmetries in the inner disc of the star V1247 Orionis. Indeed, to reproduce the 2007 and 2013 MIDI data simultaneously, we need to add a clump of dust with a size of 0.85 au. Increasing this size will imply a visibility drop that is not seen in the flat 2007 MIDI visibility. Moreover, in order to explain both the visibility drop seen in the 2013 MIDI data and the flat shape of the 2007 MIDI visibility, one is bound to place the clump at a position angle which makes it invisible to the 2007 baseline (e.g. the same position angle as that of the 2013 MIDI data). This shows that our results are very sensitive to the adopted size and position angle of the clump. To summarize, adding a spiral wave and /or a disc warping would allow us to better resolve the disc and decrease the modelled visibilities below the observed ones and increase the level of the SED up the observed ones, since these structures are more extended radially and azimuthally.

5 SUMMARY AND PERSPECTIVES

Using spectro-interferometry, we were able to resolve the circumstellar emission around the Herbig star MWC480. We performed a multiwavelength modelling which aimed at reproducing the broadband SED, the Keck and the MIDI interferometric data. The modelling is based on a semi-analytical approach using a temperature and surface density-gradient one-component disc. Our aim is to constrain the inner disc structure and in particular its axisymmetry better, as suggested by previous interferometric studies. We concluded that:

(i) an axisymmetric continuous model cannot reproduce all our data, in particular the two MIDI measurements taken at perpendicular direction and the SED for the wavelengths between 8 and 18 μm.

(ii) Fitting independently the two MIDI visibilities implied photometric changes which are not consistent with the 2007 and 2013 IR spectra.

(iii) A better agreement is obtained by considering in addition a bright feature which we determined to be located at 5.45 au from the star with a temperature of 400 K. If we assume that, in 2013, the clump is indeed aligned with the 2013 MIDI baseline, the fact that this clump is invisible to the 2007 baseline (i.e. its projected distance on to the direction of the 2007 baseline is zero) could be roughly explained in the frame of clump in Keplerian rotation.

Reconstructing images of this disc with the upcoming second-generation VLTI instrument MATISSE (the Multi AperTure mid-Infrared SpectroScopic Experiment; Lopez et al. 2006) constitutes a unique perspective to further assess the nature of the inner region of the disc around MWC480. MATISSE will recombine up to four telescopes in the mid-IR (from 3 to 13 μm) and will thus provide a more complete UV coverage with different baseline orientations and closure phase measurements, which will be used to reveal unambiguously brightness asymmetries.

ACKNOWLEDGEMENTS

The initial MIDI observation of this work has been obtained by Di Folco in 2007. We could again observe MWC480 in 2013. This work is supported at the Aerospace Corporation by the Independent Research and Development programme. NJ acknowledges the PhD financial support from the Observatoire de la Cote d'Azur and the PACA Region. The authors wish to thank C. A. Grady, A. Crida, A. Meilland, P.Tanga and S. Casassus for useful exchanges and V. Girault for helping in the 2013 observations.

REFERENCES

Akiyama E., Momose M., Kitamura Y., Tsukagoshi T., Shimada S., Koyamatsu S., Hayashi M., 2013, PASJ, 65, 123
Chapillon E. et al., 2012, ApJ, 756, 58
Chiang E. I., Goldreich P., 1997, ApJ, 490, 368
Cushing M. C., Vacca W. D., Rayner J. T., 2004, PASP, 116, 362
Dullemond C. P., Dominik C., Natta A., 2001, ApJ, 560, 957
Dutrey A., Guilloteau S., Prato L., Simon M., Duvert G., Schuster K., Menard F., 1998, A&A, 338, L63
Dutrey A. et al., 2011, A&A, 535, A104
Eisner J. A., Hillenbrand L. A., White R. J., Bloom J. S., Akeson R. L., Blake C. H., 2007, ApJ, 669, 1072
Eisner J. A., Graham J. R., Akeson R. L., Najita J., 2009, ApJ, 692, 309
Eisner J. A., Hillenbrand L. A., Stone J. M., 2014, MNRAS, 443, 1916
Grady C. A. et al., 2010, ApJ, 719, 1565
Guilloteau S., Dutrey A., Piétu V., Boehler Y., 2011, A&A, 529, A105
Hamidouche M., Wang S., Looney L. W., 2006, Bull. Am. Astron. Soc., 38, 944
Hillenbrand L. A., Hartmann L. W., 1998, ApJ, 492, 540
Huang J. et al., 2017, ApJ, 835, 231

Ingleby L., Espaillat C., Calvet N., Sitko M., Russell R., Champney E., 2015, ApJ, 805, 149
Isella A., Carpenter J. M., Sargent A. I., 2009, ApJ, 701, 260
Jaffe W. J., 2004, in Traub W. A., ed., Proc. SPIE Conf. Ser. Vol. 5491, New Frontiers in Stellar Interferometry. SPIE, Bellingham, p. 715
Jamialahmadi N., Lopez B., Berio P., Flament S., Spang A., 2014, Ap&SS
Jamialahmadi N. et al., 2015, A&A, 579, A81
Kusakabe N. et al., 2012, APJ, 753, 153
Laor A., Draine B. T., 1993, ApJ, 402, 441
Leinert C. et al., 2003, Ap&SS, 286, 73
Lopez B. et al., 2006, SPIE, 6268, 0Z
Mannings V., Koerner D. W., Sargent A. I., 1997, Nature, 388, 555
Menu J., van Boekel R., Henning T., Leinert C., Waelkens C., Waters L. B. F. M., 2015, A&A, 581, A107
Piétu V., Dutrey A., Guilloteau S., Chapillon E., Pety J., 2006, A&A, 460, L43
Piétu V., Dutrey A., Guilloteau S., 2007, A&A, 467, 163
Pringle J. E., 1981, ARA&A, 19, 137
Rayner J. T., Cushing M. C., Vacca W. D., 2009, ApJS, 185, 289
Sandell G., Weintraub D. A., Hamidouche M., 2011, ApJ, 731, 133
Simon M., Dutrey A., Guilloteau S., 2000, ApJ, 545, 1034
Sitko M. L. et al., 2007, Meteorit. Planet. Sci. Suppl., 42, 5284
Sitko M. L. et al., 2008, ApJ, 678, 1070
Thi W.-F., Woitke P., Kamp I., 2011, MNRAS, 412, 711
Vacca W. D., Cushing M. C., Rayner J. T., 2003, PASP, 115, 389
van Leeuwen F., 2007, A&A, 474, 653
Weidenschilling S. J., 1997, LPI, 28, 1517

This paper has been typeset from a TEX/LATEX file prepared by the author.